# X-Ray Photoelectron Spectroscopy of SiO<sub>2</sub>-Si Interfacial Regions: Ultrathin Oxide Films

Abstract: The composition and width of the interfacial region formed between thin thermally-grown oxide films and single-crystal Si substrates were nondestructively characterized by means of x-ray photoelectron spectroscopy. Data obtained from variations in corelevel binding energies, from variations in photoelectron line intensities, and from variations in photoelectron linewidths indicate the presence of a nonstoichiometric oxide-Si transition region. The composition and width of this region are dependent upon substrate orientation, but are invariant with change in other oxidation processing parameters. Transition regions formed on (100) oriented substrates are narrower and more completely oxidized than those formed on (111) oriented substrates. Although both Si-Si bonds and SiO-Si groups are present in this nonstoichiometric region, they do not appear to be a mixture of Si and SiO<sub>2</sub>. Instead, a continuous distribution of Si tetrahedra, Si-(O)<sub>x</sub>(Si)<sub>4-x</sub>, are formed, in which x changes from 0 to 4 as one proceeds from the substrate to the stoichiometric SiO<sub>2</sub> film.

#### Introduction

Several attempts [1–12] have recently been made to characterize the SiO<sub>2</sub>-Si interface, but the various results contain significant differences. The derived width of the interfacial region ranges from that of a near-perfect interface [6, 10, 11] to a transition region about 4.0 nm (40 Å) thick [3]. The composition of the partially oxidized transition region and the composition of SiO have been described either as containing Si- $(O)_x(Si)_{4-x}$  groups [8, 13, 14] or as mixtures of Si and SiO<sub>2</sub> [3, 15, 16]. Changes in transition region stoichiometry have been ascribed to Si protuberances, or islands, with heights of about 3.0 nm [3]. However, no evidence was found for phase separation within the amorphous oxide layer when thin cross sections of SiO<sub>2</sub>-Si were examined by transmission electron microscopy at a resolution greater than 1.0 nm [17]. The existence of a SiO<sub>9</sub>-Si transition region, its width and composition, and the parameters that alter this region, still require further clarification.

This paper extends our earlier studies [7, 18] and describes the application of x-ray photoelectron spectroscopy (XPS) as a tool for quantitative determination of nonstoichiometry in SiO<sub>2</sub>-Si interfacial regions. Analytical and chemical bonding data are both obtained from XPS [19]. As a consequence of the mean escape depths of photoelectrons, which typically are about 1.5-3.0 nm deep, XPS is ideally suited for nondestructive character-

ization of ultrathin oxide regions formed near a surface. Surface and subsurface Si oxide film composition can be derived from analysis of XPS data. The XPS photoelectron intensity data also provide a basis for measuring the widths of surface oxide regions.

Ultrathin thermally oxidized Si films were characterized by measuring changes in XPS binding energies, in photoelectron line intensities, and in linewidths as the Si oxide film thickness was changed. Analysis of the XPS data indicated the presence of a partially oxidized Si layer located in the oxide film region near the substrate. The composition and width of this transition region were evaluated primarily from binding energy data. Oxidation conditions, oxidant, substrate orientation, and substrate type were varied when preparing the oxide-Si structures. The extent to which the SiO<sub>2</sub>-Si interface was modified due to these variations in oxidation processing parameters was also investigated. Intensities and linewidths were independently used to characterize the transition region. Results from analyses of the intensity and linewidth data are consistent with corresponding binding energy results. These ultrathin oxide data form the basis for characterization of transition regions between thicker SiO<sub>2</sub> films, typically found in semiconductor devices, and oriented Si substrates. This comparison is described in detail in a subsequent paper [9].

Copyright 1978 by International Business Machines Corporation. Copying is permitted without payment of royalty provided that (1) each reproduction is done without alteration and (2) the *Journal* reference and IBM copyright notice are included on the first page. The title and abstract may be used without further permission in computer-based and other information-service systems. Permission to *republish* other excerpts should be obtained from the Editor.

#### **Experiment**

Oxide film thicknesses d were derived from ellipsometric measurements by using light at a wavelength of 546.1 nm, after careful alignment of the ellipsometer. Film thicknesses of films prepared at elevated temperatures were rapidly measured to minimize the buildup of surface contamination. The measured value of  $\Delta$  and an assumed film index of refraction n of 1.46, corresponding to  $\mathrm{SiO}_2$ , were used to evaluate film thicknesses. In the oxide thickness range under consideration, n cannot be determined from ellipsometric measurements.

An AEI ES-100 electrostatic analyzer was used to obtain photoelectron spectra. Samples were excited with Mg K $\alpha$  (1253.6 eV) radiation. Silicon [Si(2p)] and oxygen [O(1s)] binding energies, linewidths, and line intensities were recorded as a function of oxide film thickness. The Si(2p) binding energy data were referenced to the Si(2p) substrate binding energy at 99.3 eV. Photoelectron line areas were measured to obtain intensity data.

The carbon [C(1s)] line intensity was also recorded to monitor surface contamination levels. Carbon was the only contaminant detected. From variable angle XPS studies [12, 20] and from a C(1s) line intensity that is independent of oxide film thickness [18], it was concluded that the carbon contamination is located primarily at the sample surface. A carbon contamination layer thickness on a  $SiO_2$  film was estimated to be 0.2–0.3 nm. An estimated 0.5–0.6-nm carbon contamination film was found on unoxidized Si substrates [18].

## X-Ray photoelectron spectroscopy

The binding energy of an electronic level is  $E_{\rm B}=h\nu-E_{\rm K}-\phi$ , where  $h\nu$  is the energy of the x-ray excitation radiation,  $E_{\rm K}$  is the kinetic energy of the photoemitted electron as measured in the spectrometer, and  $\phi$  is a spectrometer constant. Binding energies are referenced to the Fermi level. Changes in the chemical environment about an atom cause a binding energy shift. Core electron binding energy shifts have been correlated with ligand electronegativities for a large number of compounds [19]. Hollinger

et al. [21] have noted that the chemical shifts of inner shells of Si correlate with the number of Si-O bonds in a tetrahedron such as that of  $Si-(Si)_x(O)_{4-x}$ . These shifts are related to the charge transferred between the atoms. When varying the Si tetrahedra stepwise from  $Si-(Si)_4$  to  $Si-(O)_4$ , we expect an equal change in Si(2p) binding energy for each of the four equivalent changes in composition. Some uncertainty exists in the relationship between core binding energies and chemical composition since both relaxation processes and changes in Fermi level also alter binding energies.

Photoelectron line intensities provide a basis for determining film thickness in the ultrathin film range as well as for determining atom concentrations per unit volume. The ratio of photoelectron intensity I from a film of thickness d to the intensity of pure bulk material is given by Eq. (1),

$$I_{\text{film }d}/I_{\text{film }\infty} = 1 - \exp(-d/\lambda), \tag{1}$$

where  $\lambda$ , the mean escape depth, is defined as the distance for which 1/e of the photoelectrons are not inelastically scattered [22]. The film thickness d is adjusted for the tilt in sample plane from the normal to the spectrometer analyzer entrance slit. The bulk film intensity is

$$I_{\text{film }\infty} = |KD| \exp(-d/\lambda) d\lambda = KD\lambda, \tag{2}$$

where K is constant for a particular kinetic energy and electron level, and D represents an atom density within a film and varies with film composition. The photoelectron intensity ratio for photoemitted electrons from a two-layer structure with photoelectron lines arising from the same atomic level and close in kinetic energy is

$$R = \frac{I_2[\text{Si}(2p)]_{\text{Si}}}{I_1[\text{Si}(2p)]_{\text{ox}}} = \frac{I_{2,\infty}}{I_{1,\infty}} \cdot \frac{\exp(-d/\lambda_1)}{1 - \exp(-d/\lambda_1)}, \quad (3)$$

where

$$I_{2_{\text{substrate }\omega}}/I_{1_{\text{film }\omega}} = D_2 \lambda_2/D_1 \lambda_1. \tag{4}$$

Intensity data from a two-layer structure are thus obtained in one sampling when applying Eq. (3). Errors due to variations in sample size, sample position, x-ray flux, and surface contamination are eliminated. However, accurate bulk material intensity data are required for Eq. (3) because these experimental data are subject to contamination errors. Bulk intensities were therefore calculated by using Eq. (4) for comparison with experimental data.

Photoelectron linewidths (FWHM—full width, half maximum) also provide a basis for the characterization of a film if linewidths of appropriate reference films are available. Line broadening will result from the fusion of photoelectron lines with similar binding energies but with different linewidths. Changes in bonding environments af-

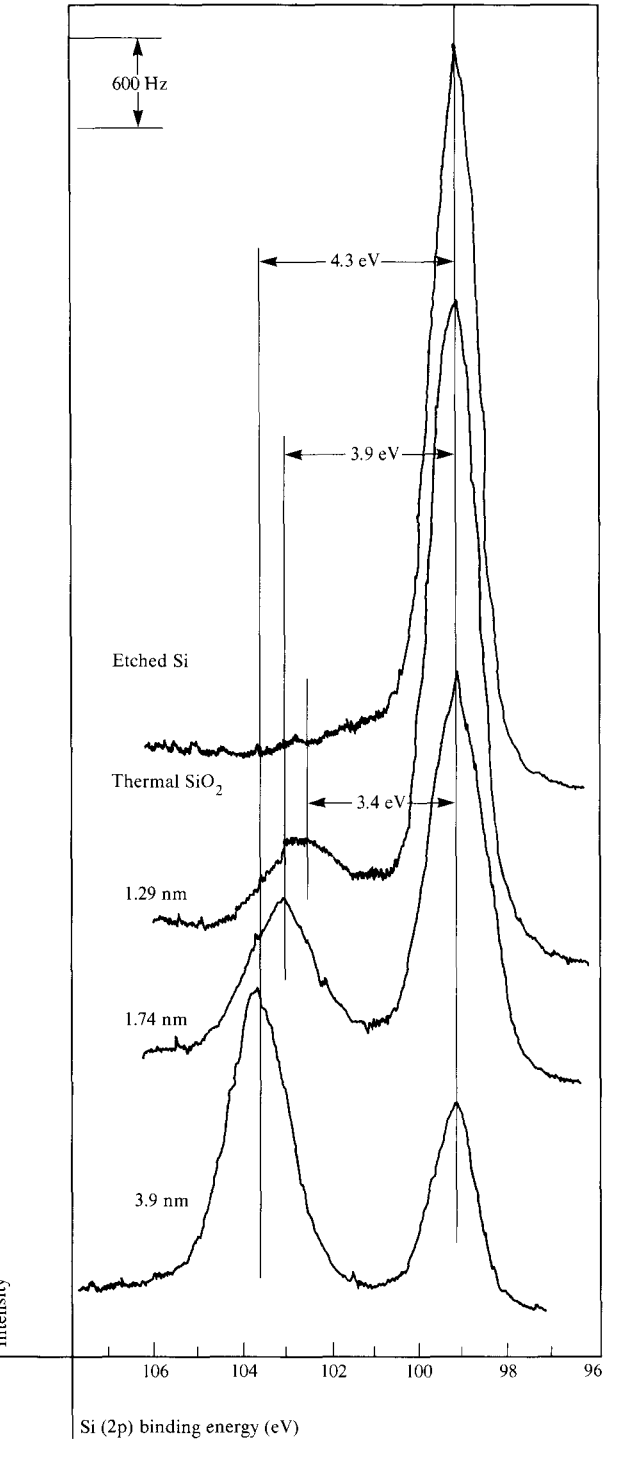
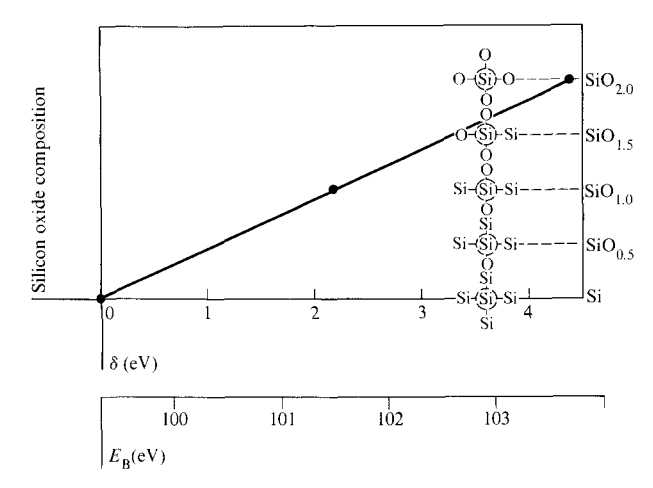


Figure 1 Si(2p) photoelectron spectra from HF-etched Si and from thermally oxidized films on  $\langle 100 \rangle$  oriented Si substrates vs oxide film thickness [7]. Photoelectrons from the substrate appear at the lower binding energies.

fect photoelectron linewidths by altering the lifetime of core-hold states that decay primarily from Auger transitions in the valence level. Core-level vacancies located immediately below the valence bands have been shown to



**Figure 2** Variation in Si(2p) binding energy  $E_{\rm B}$  with average oxide film composition [22]. Encircled Si atoms in tetrahedral configurations represent photoexcited atoms.

alter linewidths [23–25]. Species with small differences in binding energies also contribute to linewidth broadening. Contributions to photoelectron line specira are exponentially attenuated with distance from the film surface

#### Results and discussion

### • Nonstoichiometry of ultrathin silicon oxide films

The experimentally measured Si(2p) substrate binding energy remains constant at 99.3 eV for substrates with dopant concentrations  $<10^{18}$  cm<sup>-3</sup>. The value of  $E_{\rm B}[{\rm Si(2p)}]_{\rm substrate}$  is therefore used as an internal binding energy reference for the thin oxide films. The value of  $E_{\rm B}[{\rm Si(2p)}]_{\rm oxide}$  from oxide films >2.0 nm thick remains constant at 103.7 eV. The  $E_{\rm B}[{\rm Si(2p)}]_{\rm oxide}$  value decreases as the substrate is approached. Examples of Si(2p) spectra for oxide films of different thickness are shown in Fig. 1.

Changes in Si(2p) oxide binding energies, referenced to the Si(2p) substrate binding energy, are represented by  $\delta$ , where

$$\delta = E_{\rm B}[\mathrm{Si}(2\mathrm{p})]_{\mathrm{oxide}} - E_{\rm B}[\mathrm{Si}(2\mathrm{p})]_{\mathrm{substrate}}.$$
 (5)

Variations in Si oxide film stoichiometry are determined from comparisons with  $E_{\rm B}[{\rm Si}(2{\rm p})]$  data obtained from homogeneous reference compounds of varying oxygen content. Reference Si(2p) binding energies were obtained from XPS spectra of Si, SiO, and SiO<sub>2</sub> [14]. As illustrated in Fig. 2, a linear change in  $E_{\rm B}[{\rm Si}(2{\rm p})]$  is observed from changes in oxygen content of the homogeneous reference Si compounds. The relationship between Si(2p) oxide binding energies  $\delta$  and homogeneous SiO<sub>x</sub> film composition is given by  $\delta({\rm eV})=2.2~x$ .

In Fig. 3, experimentally measured shifts in  $\delta$  are compared with calculated  $\delta$  values for ideal interfaces and are plotted against ellipsometric oxide film thickness. For oxide films >2.0 nm thick,  $\delta$  is constant at 4.4  $\pm$  0.1 eV, but decreases as the oxide film is made thinner. Similar trends in Si(2p) binding energy data were previously reported [4, 5, 7, 12, 18].

An ideal interface between a Si substrate and a stoichiometric  $SiO_2$  film requires that one intermediate layer be present in which Si atoms are incompletely oxidized. The dashed curves in Fig. 3 correspond to ideal  $SiO_2$ -Si interfaces. These curves are obtained by placing a single 0.3-nm layer of  $SiO_{0.5}$ ,  $SiO_{1.0}$ ,  $SiO_{1.5}$  between the substrate and the stoichiometric  $SiO_2$  film. XPS profiles are synthesized by incrementally adding layers of oxide film to the substrate to obtain changes in  $\delta$  with changes in oxide film thickness. Gaussian-shaped photoelectron lines with linewidths of 1.3 eV and 1.8 eV from substrate and oxide, respectively, were used to obtain the XPS profiles. Line intensities were derived from Eqs. (3) and (4).

The experimental  $E_{\rm B}[{\rm Si(2p)}]$  data shown in Fig. 3 differ from the  $E_{\rm B}[{\rm Si(2p)}]$  data derived for ideal  ${\rm SiO_2}\text{-Si}$  interfacial regions. Instead, these data are consistent with the presence of a graded, incompletely oxidized oxide region near the Si substrate. The extent to which the Si atoms in this region are oxidized decreases with decreasing distance from the substrate. The experimentally obtained oxide film O(1s) binding energies, although scattered, appear unchanged both within the transition region and the stoichiometric oxide film. The chemical environment about the oxygen atoms within the transition region remains constant. Oxygen is presumably bonded as Si-O-Si groups in oxidized Si films [26].

The thicknesses of the Si oxide films plotted in Fig. 3 were derived from ellipsometric measurements. A refractive index value, corresponding to that of stoichiometric  ${\rm SiO}_2$ , was assumed to calculate ultrathin oxide film thicknesses. However, if ultrathin oxide films are nonstoichiometric, discrepancies in film thickness are introduced.

Ultrathin Si oxide film thicknesses were therefore derived from XPS intensity data. Contributions to XPS intensity data are exponentially attenuated with distance from the film surface. Mean escape depths  $\lambda$  were evaluated [7] from Eqs. (3) and (4), which relate Si(2p) intensity data to oxide film thicknesses. Values of  $\lambda$  for Si(2p) photoelectrons emitted from the oxide and from the substrate are 2.5 nm and 2.3 nm, respectively, when a Mg K $\alpha$  x-ray source is used. These  $\lambda$  values were derived for Si-Si oxide structures with oxide films >2.0 nm thick. The bulk film intensity ratio of 1.95 used in Eq. [3] is consistent with the calculated intensity ratio of 2.0 derived from Eq. [4]. Other measurements [12] and theoretically estimated values [27] of the Si(2p) mean escape depth exist for photoelectrons emitted from Si and from

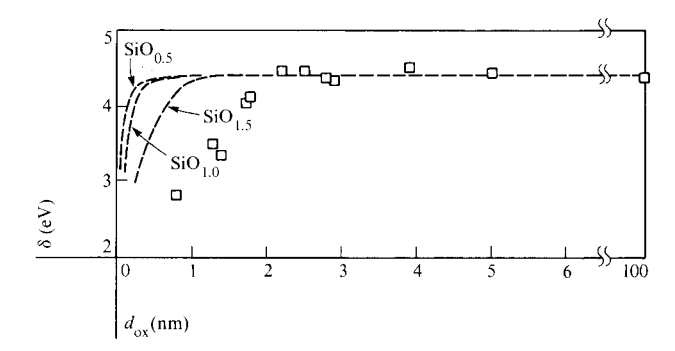


**Figure 3** Chemical shifts of the oxide Si(2p) binding energies referenced to the substrate binding energy  $\delta$  vs oxide film thickness  $d_{\rm ox}$ . The dashed curves represent calculated  $\delta$  values for ideal interfacial regions composed of one 0.3-nm layer of either SiO<sub>0.5</sub>, SiO<sub>1.0</sub>, or SiO<sub>1.5</sub>.

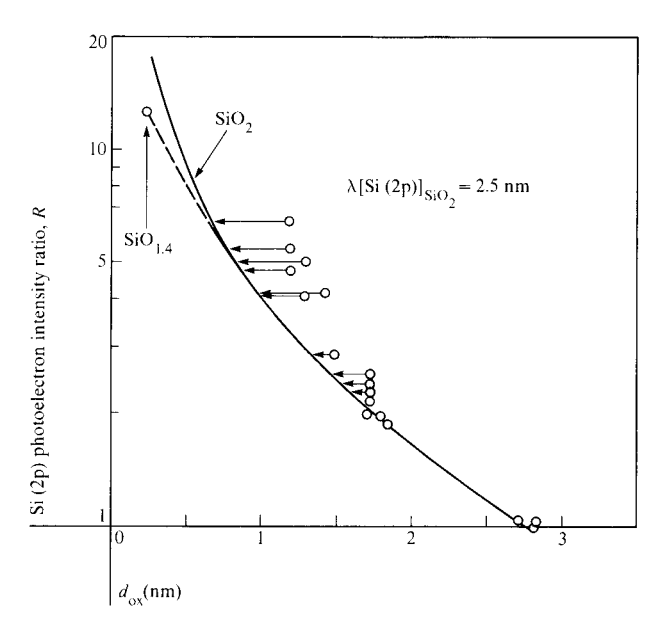
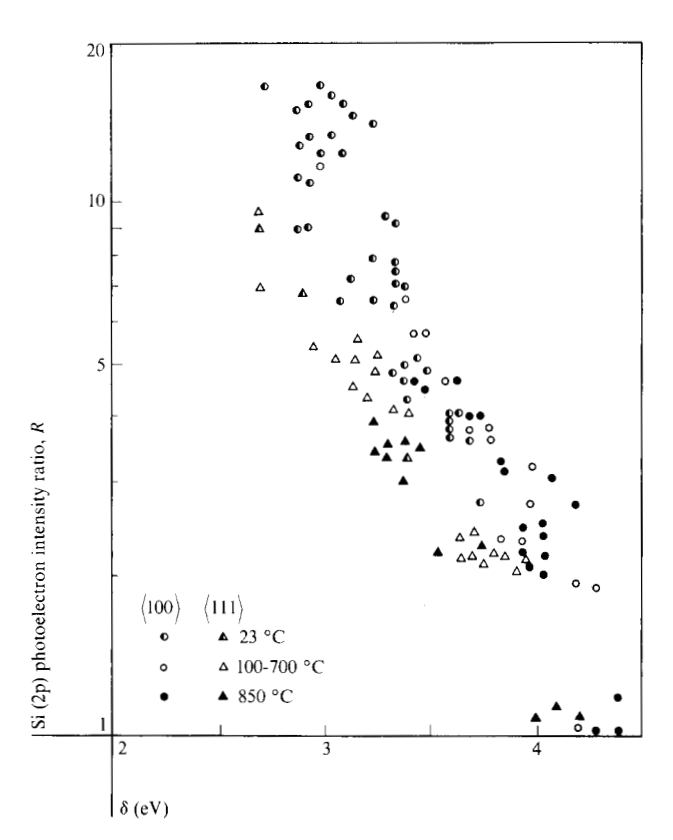


Figure 4 Intensity ratio R of Si photoelectrons from the Si substrate relative to a thermal oxide film extended, using Eq. (3), to  $\mathrm{SiO}_2$  film thicknesses  $d_{\mathrm{ox}}$  of <3.0 nm. The dashed curve represents a graded nonstoichiometric oxide film region whose average composition at  $d_{\mathrm{ox}}=0.25$  nm is  $\mathrm{SiO}_{1.4}$ .

the oxide film. Agreement for  $\lambda[Si(2p)]_{Si}$  is good and for  $\lambda[Si(2p)]_{axide}$  is fair.

In Fig. 4, the 2.5-nm Si(2p) mean escape depth curve [7] is extended into the oxide film region for film thicknesses of <3.0 nm. Intensity data from oxide films <2.0 nm thick do not fall on the curve plotted in Fig. 4 or on any single mean escape depth curve. Incompletely oxidized Si shifts the mean escape depth curve to lower intensity ratios. As discussed below, the deviations of the Si(2p) substrate to Si(2p) oxide photoelectron line in-



**Figure 5** Experimental Si(2p) intensity ratio R vs Si(2p) binding energy data  $\delta$  for oxide films grown on (111) and (100) oriented substrates.

tensity ratio R from the mean escape depth curve provide additional supporting evidence for nonstoichiometry in ultrathin oxide films.

#### • Formation of ultrathin oxide films

A more complete examination of variations in XPS data was prompted by the dissimilarity between experimental  $E_{\rm R}$  data and  $E_{\rm R}$  data calculated for ideal SiO<sub>2</sub>-Si interfaces (Fig. 3). In addition, XPS intensity (Fig. 4) and linewidth data [7] exhibit corresponding variations within the same thickness range. These variations are each consistent with the presence of a nonstoichiometric transition region. Various processing conditions were therefore used to thermally grow ultrathin oxide films on Si substrates and these were examined with regard to how they affect the SiO<sub>a</sub>-Si transition region. Experimental data are plotted in terms of Si(2p) oxide binding energy shifts referenced to the Si(2p) substrate binding energy  $\delta$  and Si(2p) intensity ratios R. Figure 2 shows that  $\delta$  is related to film composition, and Fig. 4, that R is related to film thickness. Plots of  $\delta$  vs R describe changes in composition with oxide film thickness.

Ultrathin oxide data are arbitrarily grouped according to the oxidation temperature range used. Figure 5 shows Si(2p) binding energy and intensity data that are obtained

from oxides formed at room temperature. The oxidation parameters were previously described [18]. These include oxidations in air and in water, using n- and p-type substrates with primarily  $\langle 100 \rangle$ , but also  $\langle 111 \rangle$ , substrate surface orientations. Film thicknesses were <1.3 nm. Very thin films are formed under these oxidation conditions. However, Si(2p) line resolution errors increase as the intensity of the Si(2p) oxide line decreases and as  $E_{\rm B}[{\rm Si(2p)}]_{\rm oxide}$  approaches  $E_{\rm B}[{\rm Si(2p)}]_{\rm substrate}$ . These room temperature data appear independent of processing conditions. The continuous decrease in  $\delta$  with increase in R indicates that the oxygen deficiency in the film increases as the substrate is approached.

Additional Si(2p) data, obtained from spectra of etched Si oxidized in  $O_2$  or  $O_2/N_2$  ambients at 850°C, are shown in Fig. 5. In some cases, oxide films were annealed after oxidation in  $N_2$  at 850°C. The minimum oxide film thickness in this group of ultrathin films that could be obtained at these oxidation temperatures was about 1.1 nm as calculated from ellipsometric data. The XPS data are scattered and, except for differences due to substrate orientation, appear to be independent of processing conditions. Oxides grown on  $\langle 100 \rangle$  oriented substrates have higher binding energies ( $\delta$  values) for given Si(2p) intensity ratios (R) than data obtained from oxides formed on  $\langle 111 \rangle$  oriented substrates. The data obtained at 850°C are "thick" film extensions of data obtained at room temperature.

Also plotted in Fig. 5 are Si(2p) binding energy and intensity data from oxide films thermally grown at oxidation temperatures ranging between 100 and 700°C. On (100) oriented substrates, oxide films were formed in dry O<sub>2</sub>, generally for about half an hour, although oxidation times were varied in some cases. Data obtained from substrates oxidized in boiling aqueous solutions [H<sub>2</sub>O, HNO<sub>2</sub>, H<sub>2</sub>O<sub>2</sub>(30 percent)] for one hour are also included in Fig. 5. The XPS data from oxide films thermally grown on (100) oriented substrates were not resolvable in terms of oxidation temperature, oxidation time, or oxidant. Anomalously high ellipsometric film thicknesses were often measured after oxidation in boiling water. However, oxide film thicknesses estimated from the mean escape depth curve were <1.8 nm. A broadened Si(2p) oxide peak, sometimes detected after oxidation in boiling water, was also observed by Clarke et al. [4].

In addition, XPS data were obtained from spectra of etched Si oxidized at 600°C in dry  $O_2$  from oxide films formed on  $\langle 111 \rangle$  oriented substrates. As previously observed, the XPS data for oxides grown on  $\langle 100 \rangle$  oriented substrates are of higher binding energies for given Si(2p) intensity ratios than are corresponding data from oxides formed on  $\langle 111 \rangle$  oriented substrates at a given film thickness.

The data shown in Fig. 5 are scattered but form two distinct groupings that are associated only with dif-

ferences in substrate orientation. Within each group, a decrease in Si(2p) oxide binding energies is observed with a decrease in Si(2p) intensity ratio. This corresponds to a reduction in oxide film oxygen content as the substrate is approached. This nonstoichiometric transition region is oxygen-deficient near the SiO2 surface and becomes less oxidized as the Si surface is approached. No distinct Si(2p) lines that would correspond to one or more unique oxidized Si compounds are detected in any of our spectra. The Si(2p) photoelectrons from the oxide film cannot be deconvoluted into lines corresponding to a mixture of Si and SiO, [28]. Instead, the transition region composition is best represented by a distribution of tetrahedral configurations ranging from Si-(Si), in the substrate to Si-(O), in stoichiometric SiO<sub>2</sub> (Fig. 2). For a given film thickness within this nonstoichiometric film thickness region, oxides formed on (100) oriented substrates are more completely oxidized than are oxides formed on (111) oriented substrates. Similar results have been obtained from XPS analysis of transition regions between thicker, thermally grown oxide films (≤100.0 nm thick) and oriented Si substrates [9].

• Analysis of Si(2p) binding energy and intensity data Experimental data presented in Fig. 5 are analyzed by using a simple procedure to synthesize XPS profiles. Nonstoichiometric transition regions are subdivided into layers L, each 0.25 nm thick. The average composition of the first transition region layer L(1) beyond the Si substrate is characterized as follows. From Eq. (3), the intensity ratio R is evaluated for  $d = SiO_9$ , film 0.25 nm thick. A value of the Si(2p) oxide binding energy  $\delta$  is obtained from Fig. 5 by extrapolating the experimental data to an intensity ratio R, corresponding to a SiO<sub>2</sub> film 0.25 nm thick. By using this δ value, the composition of this first layer is derived from Fig. 2, which relates  $\delta$  to SiO<sub>x</sub> composition. A single iteration in this procedure is used to adjust the value of R for oxide nonstoichiometry by altering  $D_1$  in Eq. (4).

The number of additional layers of nonstoichiometric oxide film 0.25 nm thick present within a transition region is then estimated. It is assumed that a) there exists a linear gradation between L(1) and the stoichiometric  $SiO_2$  film, and b) an addition of a new layer does not alter the average composition of the underlying layers. The shape of the photoelectron peak intensity for each layer is approximated by a Gaussian distribution. Contributions of each additional layer to the total oxide intensity are calculated by using Eq. (3). Substrate and oxide layer linewidths (FWHM) are 1.3 eV and 1.8 eV, respectively. The average composition of each layer is derived from the Si(2p) oxide binding energy  $\delta[L(i)]$ , obtained from Fig. 2. The transition region is then subdivided into layers with specified oxide compositions. Nonstoichiometric and

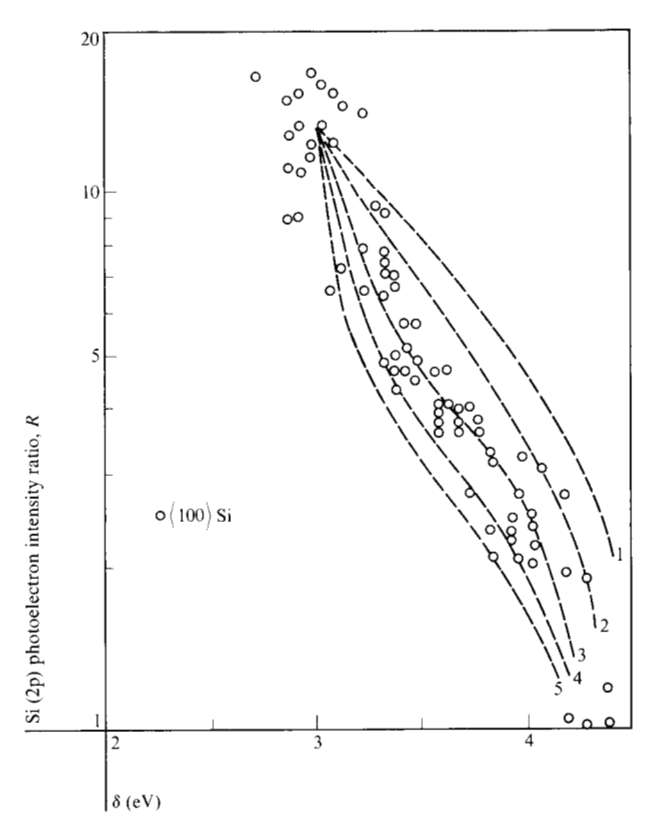


Figure 6 Comparison between experimental data from oxide films grown on  $\langle 100 \rangle$  oriented Si substrates and calculated (dashed) curves obtained for SiO<sub>2</sub>-Si structures. The numbers associated with the dashed curves represent the number of 0.25-nm layers in the calculated transition regions.

stoichiometric oxide layers are added incrementally to derive the change in  $\delta$  vs R. The transition region width is then changed and this procedure is repeated. A series of curves are generated with different transition region compositions and widths. The best fit between the experimental data in Fig. 5 and the generated curves is used to derive an estimate of  $SiO_2$ -Si transition region width and composition.

• Transition region composition and width from  $E_{\rm B}$  data Experimental data shown in Fig. 5 are grouped according to substrate orientation. The  $\langle 100 \rangle$  data are extrapolated to a layer 0.25 nm thick that has an average composition of SiO<sub>1.4</sub>. The estimated transition region width on the  $\langle 100 \rangle$  Si substrate, determined from comparing experimental data with the generated curves, is about 0.75 nm thick (Fig. 6). Similarly, the  $\langle 111 \rangle$  data are extrapolated to an initial layer 0.25 nm thick that has an average composition of SiO<sub>1.2</sub>. The transition region width, determined by comparing experimental data with the generated curves, is estimated to be about 1.0 nm thick (Fig. 7). These results are summarized in Fig. 8 and represent a

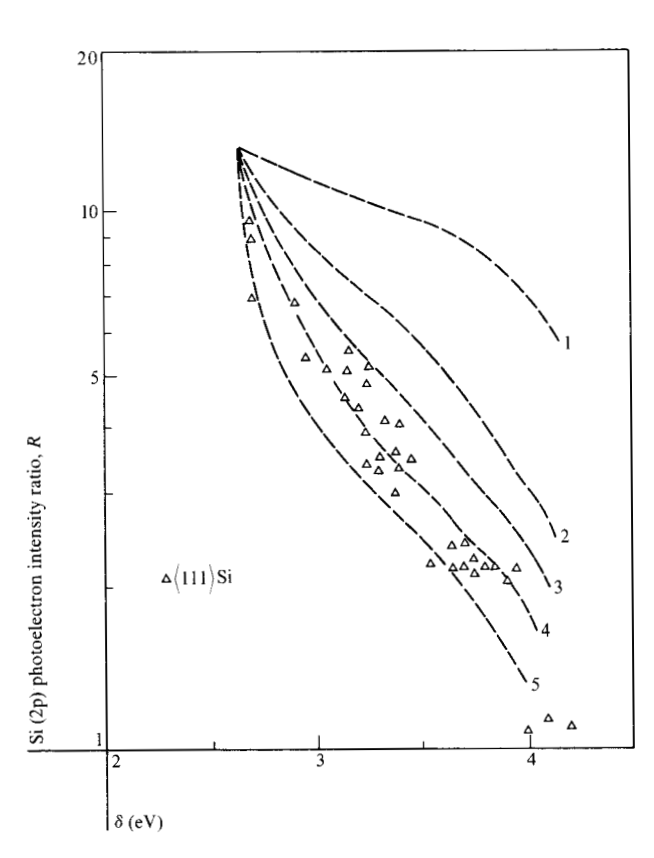


Figure 7 Comparison between experimental data from oxide films grown on (111) oriented Si substrates and calculated (dashed) curves obtained for SiO<sub>2</sub>-Si structures. The numbers associated with the dashed curves represent the number of 0.25-nm layers in the calculated transition regions.

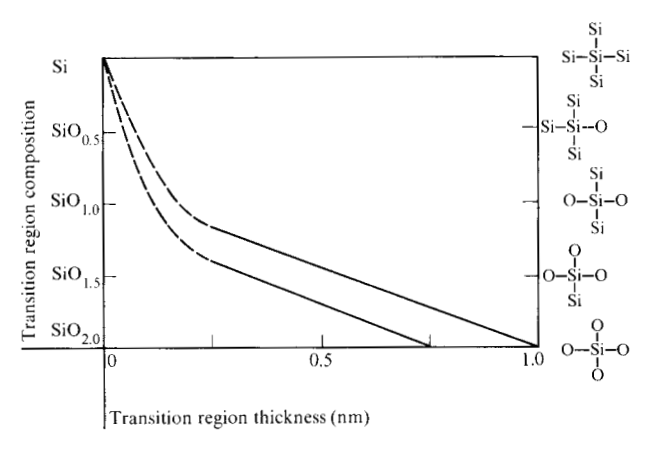


Figure 8 Transition region composition and width derived from ultrathin oxide Si(2p) binding energy and intensity data.

refinement of earlier results [8]. The transition region on  $\langle 100 \rangle$  oriented substrates possesses an estimated 0.8  $\times$  10<sup>15</sup> unoxidized Si-Si bonds cm<sup>-2</sup>. On  $\langle 111 \rangle$  oriented substrates, this region contains about 1.4  $\times$  10<sup>15</sup> unoxidized Si-Si bonds cm<sup>-2</sup>.

#### Linewidth data

In Fig. 9, the oxide Si(2p) and O(1s) linewidths, obtained from oxides grown at elevated temperatures on (100) oriented Si substrates, are plotted vs oxide film thickness. An increase in both O(1s) and Si(2p) oxide linewidths (FWHM) is observed with a decrease in film thickness for films <2.5 nm thick. For thicker oxide films, a constant minimum photoelectron linewidth is detected for both of these lines. The Si(2p) substrate linewidth (not shown) remains constant and is independent of film thickness. Broadened photoelectron lines can result from changes in the lifetimes of core-hole states as well as from the fusion of lines obtained from a distribution of species with small differences in binding energies. As a first-order approximation, it is assumed that linewidths change linearly with oxygen content in the oxide film. Reference linewidth data are obtained from SiO (2.3 eV) and from SiO<sub>a</sub> (1.8 eV) samples [7, 14]. In Fig. 9, a Si(2p) linewidth comparison is made between experimental data obtained from oxide films grown on (100) oriented substrates and calculated linewidths. Calculated transition region widths range from 2 to 5 layers, each 0.25 nm thick. The convolution procedure described earlier is adjusted to account for the change in linewidth with oxide film composition. The experimental data are best fitted to a three-layer transition region. This is in agreement with chemical bonding variations in Si oxide films <2.5 nm thick derived from  $E_{\rm p}[{\rm Si}(2{\rm p})]$  data. A comparison between O(1s) experimental data and a curve derived for a three-layer transition region is also shown in Fig. 9.

#### ♦ Analysis of oxide O(1s)/Si(2p) intensity data

The atom density term D in Eq. (2) changes as the oxide film composition changes. The O-to-Si intensity ratio of photoemitted electrons from the oxide film therefore provides an additional measure of film composition. These intensity data are independent of possible discontinuities in the oxide films and represent an average contribution only from the oxide films. Oxygen and Si intensities are determined from Eqs. (1) and (2), and the O-to-Si intensity ratio is given by

$$\frac{I_{1}[O(1s)]}{I_{2}[Si(2p)]_{ox}} = \frac{K_{1}D_{1}\lambda_{1}}{K_{2}D_{2}\lambda_{2}} \cdot \frac{1 - \exp(-d/\lambda_{1})}{1 - \exp(-d/\lambda_{2})}$$
(6)

and

$$\frac{I_1[\mathrm{O}(1\mathrm{s})]_{\infty}}{I_2[\mathrm{Si}(2\mathrm{p})]_{\infty,\mathrm{ox}}} = \frac{K_1 D_1 \lambda_1}{K_2 D_2 \lambda_2}.$$
 (7)

Mean escape depth curves are calculated from the intensity data for oxide films >2.0 nm thick by using Eqs. (6) and (7) with  $I_1[O(1s)]_{\infty}/I_2[Si(2p)]_{\infty} = 0.27$  nm,  $\lambda_1[O(1s)] = 1.6$  nm,  $\lambda_2[Si(2p)]_{\text{oxide}} = 2.5$  nm,  $D_1 = 1.21$  g cm<sup>-3</sup> and  $D_2 = 1.06$  g cm<sup>-3</sup>.

An ideal  $\mathrm{SiO_2}$ -Si interface must possess one layer of Si tetrahedra with asymmetric chemical environments. In Eqs. (6) and (7)  $D_1$  and  $D_2$  are altered to account for changes in oxide composition within the transition region. In Fig. 10, the oxide  $\mathrm{O}(1\mathrm{s})/\mathrm{Si}(2\mathrm{p})$  intensity ratio is plotted vs oxide film thickness. For  $\langle 100 \rangle$  oriented Si substrates, a one-layer interface is represented as a 0.25-nm layer of  $\mathrm{SiO}_{1.4}$  and is shown as the top curve in Fig. 10. Other curves are obtained for  $\langle 100 \rangle$  Si with transition regions 0.50 nm, 0.75 nm, and 1.00 nm thick. These curves are compared with the transition region derived from  $E_{\mathrm{n}}[\mathrm{Si}(2\mathrm{p})]$  data.

These experimental O(1s)/Si(2p) intensity data have the disadvantage of being sensitive to surface contamination. Samples exposed to air and kept in the light were generally found to have higher oxygen impurity levels than samples stored in the dark. Many of the data shown in Fig. 10 were selected after oxidation or annealing within the XPS vacuum system at temperatures to 400°C to minimize the concentration of adsorbed oxygenated impurities. O(1s) intensity data obtained from samples exposed to air generally decreased upon annealing at elevated temperatures. Film thicknesses were estimated both from ellipsometric data and from Si(2p) intensity data extrapolated to the mean escape depth curve in Fig. 4. The oxide intensity data shown in Fig. 10 appear consistent with the presence of a transition region whose composition is similar to that obtained from  $E_{\rm B}$  analysis. This consistency is, at best, qualitative because of the small difference in oxygen content between stoichiometric and nonstoichiometric films, the inability to determine whether impurities are completely desorbed from the surface, and the scatter in the experimentally obtained intensity data. These data, which are independent of possible film discontinuities, also indicate that a nonstoichiometric interfacial layer does exist.

# • Oxide nonstoichiometry from Si(2p) intensity data In Fig. 4, Si(2p) intensity data are plotted against ellipsometric film thicknesses for films <3.0 nm thick. The solid

mean escape depth curve obtained from Eq. (3) for oxide films >2.0 nm thick is extended into the thinner film region. A point corresponding to a film 0.25 nm thick with a composition of SiO<sub>1.4</sub> was calculated by adjusting D in Eqs. (3) and (4). This is plotted in Fig. 4 to illustrate the effect that a variation in oxide film composition has on displacing the SiO<sub>2</sub> mean escape depth curve. The dashed curve in Fig. 4 represents the change in the mean escape depth curve for a graded nonstoichiometric Si oxide film about 0.75 nm thick. It is apparent from Fig. 4 that Si intensity ratio data R are not strongly dependent upon film composition. The intensity data plotted vs film thicknesses in Fig. 4 do not correspond to the stoichiometric SiO<sub>2</sub> (solid curve) or to the incompletely oxidized Si (dashed curve).

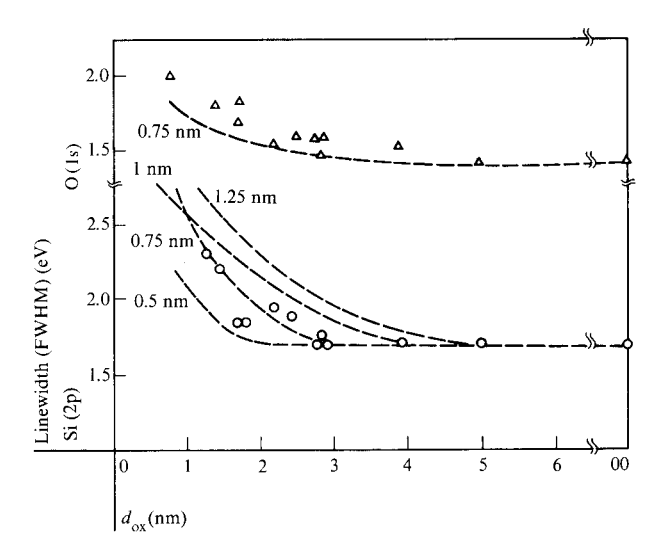


**Figure 9** Oxide Si(2p) and O(1s) linewidths (FWHM) vs oxide film thickness  $d_{\rm ox}$  from films on  $\langle 100 \rangle$  oriented substrates. The dashed curves represent calculated linewidths for graded transition regions 0.50, 0.75, and 1.00 nm thick with an initial 0.25-nm layer composition of SiO<sub>1.4</sub>.

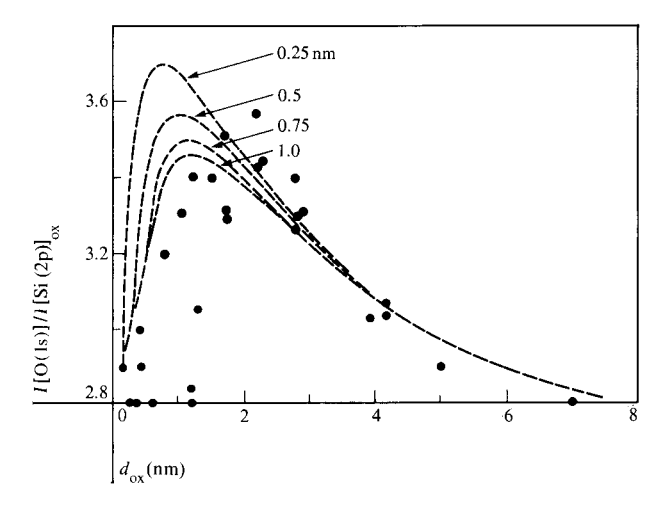


Figure 10 Oxide O(1s)/Si(2p) intensity ratio vs oxide film thickness  $d_{\rm ox}$  from films grown on  $\langle 100 \rangle$  oriented substrates. Dashed curves are calculated for graded transition regions 0.25, 0.50, 0.75, or 1.00 nm thick with an initial 0.25-nm layer composition of SiO<sub>1.4</sub>.

In Fig. 4, ellipsometric thicknesses of oxide films <2.0 nm thick are decreased in thickness for Si(2p) intensity data to correspond with the mean escape depth curve. The magnitude of the required adjustments in film thickness increases as the Si substrate is approached (Fig. 4). These data could have also been adjusted to the mean escape depth curve by a vertical displacement. The latter adjustment would correspond to the presence of a significant amount of excess unoxidized Si within the transition

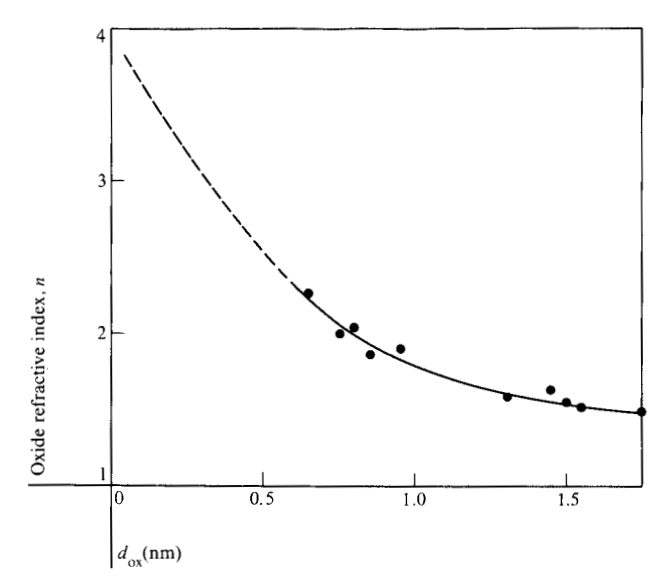


Figure 11 Oxide refractive indices n vs adjusted film thickness  $d_{\text{ox}}$  derived by using Fig. 3. Dashed portion of curve represents extrapolation to Si substrate refractive index.

region in oxide films ≥1.1 nm thick. Electron microscopy studies exhibit no evidence of oxide phase separation for oxide film thicknesses of about 1.0 nm [17]. The similarity in XPS data obtained over the range of oxidation conditions used to prepare these films also suggests that oxide discontinuities or nonuniformities are probably not major contributors to the intensity data. In addition, analyses of oxide O(1s)/Si(2p) intensity data, which are independent of possible oxide film discontinuities, are in good agreement with analyses of binding energy and linewidth data. The latter data can be affected by oxide discontinuities.

Decreasing the oxide film ellipsometric thickness in Fig. 4 corresponds to increasing the refractive index n of the oxide film. Increases in n are consistent with decreases in oxygen content of the oxide films. By assuming zero absorptivity within the transition region film, refractive indices are derived from film thicknesses by displacing the thickness data to the mean escape depth curve (Fig. 11).

A graded film may be treated as a multilayered structure with values of n corresponding to the average composition of the partially oxidized layers [29]. The changes in oxide refractive index at the  $\mathrm{SiO}_2$ -Si interface were approximated by using a multilayered structure [30] based on interface composition derived from  $E_{\mathrm{B}}$  data. These results are qualitatively consistent with refractive indices, plotted in Fig. 11, that are derived from ellipsometric and  $\mathrm{Si}(2\mathrm{p})$  intensity data (Fig. 4).

### Summary

Ultrathin Si oxide films thermally grown on oriented Si substrates were analyzed from XPS data in order to non-

destructively characterize the  $SiO_2$ -Si interfacial region. Variations in Si(2p) binding energies, Si(2p) and O(1s) intensity data, and Si(2p) oxide and O(1s) linewidths were examined over similar 2.0-2.5-nm film thickness ranges. These data indicate that a transition region extends between stoichiometric  $SiO_2$  and the crystalline Si substrate. This conclusion is supported by the quantitative agreement obtained from analysis of  $E_B[Si(2p)]$  and of linewidth data for the composition and width of the transition region, as well as by the qualitative consistency obtained from analysis of photoelectron intensity data. No single alternative interpretation is consistent with these XPS data.

Only the substrate orientation affects the interfacial region. The transition region present on (111) oriented substrates is estimated to be 1.0 nm thick and possesses Si atoms in lower oxidation states than the 0.75-nm-thick transition region present on (100) oriented substrates. For a particular substrate orientation, transition regions between stoichiometric oxide films and oriented Si substrates remain invariant. The composition and width of these regions are unaffected by changes in oxidation conditions or oxidant, or by high temperature annealing.

#### Acknowledgments

The authors thank F. W. Anderson and W. A. Pliskin for helpful comments and L. E. Forget, F. Hoey, and M. J. Palmer for their excellent technical assistance.

#### References and notes

- T. W. Sigmon, W. K. Chu, E. Lugujio, and J. W. Mayer, *Appl. Phys. Lett.* 24, 105 (1974).
- W. L. Harrington, R. E. Honig, A. M. Goodman, and R. Williams, Appl. Phys. Lett. 27, 644 (1975).
- J. S. Johannessen, W. E. Spicer, and Y. E. Strausser, J. Appl. Phys. 47, 3028 (1976).
- R. A. Clarke, R. L. Tapping, M. A. Hopper, and L. Young, J. Electrochem. Soc. 122, 1347 (1975).
- G. Hollinger, Y. Jugnet, P. Pertosa, and Tran Minh Duc, Chem. Phys. Lett. 36, 441 (1975).
- 6. H. Ibach and J. E. Rowe, Phys. Rev. B 10, 710 (1974).
- R. Flitsch and S. I. Raider, J. Vac. Sci. Technol. 12, 305 (1975).
- S. I. Raider and R. Flitsch, J. Vac. Sci. Technol. 13, 58 (1976).
- 9. S. I. Raider, R. Flitsch, and R. Rosenberg, to be published.
- 10. J. Maserjian, J. Vac. Sci. Technol. 11, 996 (1974).
- 11. T. H. DiStefano, J. Vac. Sci. Technol. 13, 856 (1976)
- J. M. Hill, D. G. Royce, M. Mehta, C. S. Fadley, L. F. Wagner, and F. J. Grunthaner, J. Vac. Sci. Technol. 14, 376 (1977).
- 13. H. R. Phillip, J. Phys. Chem. Solids 32, 1935 (1971).
- S. I. Raider and R. Flitsch, J. Electrochem. Soc. 123, 1754 (1976).
- 15. R. J. Temkin, J. Non-Cryst. Solids 17, 215 (1975).
- G. Hollinger, Y. Jugnet, and Tran Minh Duc, Solid State Commun. 22, 277 (1977).
- J. Blanc, C. J. Buiocchi, M. S. Abrahams, and W. E. Ham, Appl. Phys. Lett. 30, 120 (1977).
- S. I. Raider, R. Flitsch, and M. J. Palmer, J. Electrochem. Soc. 122, 413 (1975).

- K. Siegbahn, C. Nordling, A. Fehlman, R. Norberg, K. Hamrin, J. Hedman, G. Johansson, T. Bergman, S.-E. Karlsson, and I. Lindberg, ESCA-Atomic, Molecular and Solid State Structure Studied by Means of Electron Spectroscopy, Almquist and Wiksells, Uppsala, Sweden, 1967.
- S. I. Raider, R. Flitsch, J. A. Aboaf, and W. A. Pliskin, J. Electrochem. Soc. 123, 560 (1976).
- G. Hollinger, J. Tousset, and Tran Minh Duc, Tetrahedrally Bonded Amorphous Semiconductors, M. H. Brodsky, S. Kirkpatrick, and D. Weatre, eds., American Institute of Physics, New York, 1974, p. 102.
- 22. T. A. Carlson and G. E. McGuire, J. Electron Spectrosc. Relat. Phenom. 1, 161 (1972).
- R. W. Shaw and T. D. Thomas, Phys. Rev. Lett. 29, 689 (1972).
- R. M. Friedman, J. Hudis, and M. L. Perlman, *Phys. Rev. Lett.* 29, 692 (1972).
- 25. P. H. Citrin, Phys. Rev. Lett. 31, 1164 (1973).
- L. Spialter and J. S. Smith II, "Decomposition of Organometallic Compounds to Refractory Ceramics and Metal Al-

- loys," Proceedings of the 1967 International Symposium, University of Dayton Press, Dayton, OH, 1968, p. 195.
- 27. D. R. Penn, J. Vac. Sci. Technol. 13, 221 (1976).
- S. I. Raider, R. Flitsch, and J. M. Baker, unpublished results.
- F. Abeles, in *Ellipsometry in the Measurement of Surfaces and Thin Films*, Symposium Proceedings, Washington, 1963, E. Passaglia, R. R. Stromberg, and J. Kruger, eds., Nat. Bur. Stand. Misc. Publ. 256, 1964, p. 41.
- 30. W. R. Hunter, private communication.

Received May 3, 1977; revised October 11, 1977

S. I. Raider is located at the IBM Thomas J. Watson Research Center, Yorktown Heights, New York 10598; R. Flitsch is located at the IBM System Products Division laboratory, East Fishkill (Hopewell Junction), New York 12533.